Diyala Journal of Engineering Sciences

Journal homepage: https://djes.info/index.php/djes

ISSN: 1999-8716 (Print); 2616-6909 (Online)

Experimental and Finite Element Analysis of Deep Curved Box Girders: Impact of Concrete Strength and Geometry

Asala Asaad Dawood[1*], Khattab Saleem Abdul-Razzaq [2] and Wael Shawky Abdulsahib[1]

[1]Department of Civil Engineering, University of Technology, Baghdad, Iraq
[2] Department of Civil Engineering, University of Diyala, 32001 Diyala, Iraq

ARTICLE INFO

Article history:
Received January 15, 2024
Revised July 31, 2024,
Accepted August 29, 2024
Available online December 1, 2024

Keywords:
Continuous Bridges
Curved Box Girder
Reinforced Concrete
Finite Element
ABAQUS
Torsion

ABSTRACT

Reducing the ratio of box girders' span to their height reduces bending moments and makes them deep members that are controlled by shear behavior. The presence of horizontal curvature generates torsional moments and different deflection between the outer and inner web as a result of twisting. Two experimental specimens with the same dimensions were cast and tested, one straight and the other horizontally curved. The two specimens were numerically modeled using the ABAQUS software for the purpose of verifying the numerical model to study more parameters. The finite element analysis showed a good agreement with the experimental values with a difference of (98-99) %, (94-97)% and 103% of the experiment for ultimate loading, deflection and twisting angle, respectively. It also showed stress paths that match the experimental and theoretical results that explain the behavior of deep beams, such as the Strut and Tie method (STM). The effect of compressive strength, whole width, and the width of the bearing and supporting plates was studied. Results showed that increasing the concrete's compressive strength by about 40-120%, increased the load capacity and decreased its deflection by approximately 6-14% and 3-15%, respectively. The deep box section torsional resistance increased when its width was increased by approximately 17–50%, although this had no significantly affect on the load capacity level. A reduction of 17-33% in the width of the loading and supporting bearing plates caused a 6-16% drop in load capacity besides a notable decrease in stiffness.

1. Introduction

Horizontally curved box girders are found in bridges, overpasses, and turns. Continuous horizontal curved box girder bridges are used for their efficiency and economy compared to segmental box girder. The importance of curved bridges has increased due to development, crowding, and limited spaces allocated for construction [1, 2]. In the horizontally curved girder, unlike a straight girder, the neutral axis and the centroidal axis are not coincident of a horizontal curved girder, so torsional moments occur. Furthermore, due to high depth, stresses do not vary linearly from the neutral axis [3, 4]. When there is no torsion present in straight concrete girders, the cross-sectional deflection remains constant across the girders' width. On the other hand, torsion leading to twisting occurs in straight concrete girders and curved concrete girders that are eccentrically loaded. As a result, the cross-section’s deflection varies along the girder width, with the largest deflection typically occurring at the section's extreme inner or outer edge. According to the AASHTO

* Corresponding author.
E-mail address: asalaasaad01@gmail.com
DOI: 10.24237/djes.2024.17407

LRFD Bridge Design Specification, for horizontally curved concrete girders, the curvature induces twisting. Concrete box girder superstructures with horizontal curvature that satisfy the requirement of having a central angle within one span ranging from 12 to 34 degrees can be examined as single-spine beams made up of straight segments, as long as no segment has a central angle greater than 3.5 degrees [5]. An adequate three-dimensional model of the structure must be employed for integral substructures. It is necessary to account for the redistribution of forces caused by the concrete's time-dependent characteristics.

When compared to open section girder bridges, concrete box bridges offer noticeably higher torsional stiffness in addition to their low material content, relative light weight, and strong flexural rigidity [6-10].

Higher-depth curved members are necessary to carry high loads and to satisfy certain aesthetic requirements. In comparison to shallow members, deep members are structural members with a greater depth and a thickness that is substantially less than both depth and span [11]. The deep beam is defined differently depending on the adopted code. When the effective span length (L) to overall depth (h) of a beam's is less than 2.5 for continuously supported beams and less than 2 for simply supported beams, respectively, the beam is classified as a deep beam. To put it another way, a beam is considered deep if its clear span (ln) are equal to or less than four times h, or if its regions of concentrated loads are located within twice h from the support face [12]. Deep beams differ from shallow beams in that they are unable to distinguish in terms of uniaxial stress-strain characteristics due to the nonlinear strain distribution across the depth [13-18]. Furthermore, the situation is made more complex by the nonhomogeneous character of the materials involved.

Compared to simply supported deep beams, continuous deep beams behave very differently. The development of cracks in continuous deep beams is significantly affected by the presence of high shear and high moment within the interior shear span. This results in a notable decrease in the effective strength of the concrete strut, which serves as the primary load transmission element in deep beams. Deep members are analyzed and designed using the STM for its efficiency in explaining their behavior. The STM consists of compression members called struts and tensile members called ties, connected together by nodes to form a truss-like system through which the stresses resulting from the applied loads are transmitted. STM has become approved in most international codes [19].

In large cities and modern highway systems, box girder bridges with a horizontal curvature have gained popularity recently. While a great deal of study has been conducted to investigate and understand the behaviour of various types of box-girder bridges, the findings from these studies are dispersed and require evaluation. Because modern highway bridges are frequently subject to severe geometric restraints in urban areas where elevated highways and multi-level structures are necessary, the use of straight segmental construction has decreased relative to curved girders. As a result, the bridges must be constructed as a curved alignment.

Since there are fewer intermediate supports, expansion joints, and bearing details, the overall cost of the curved girder system has decreased dramatically, even though the cost of creating the superstructure as a curved girder is higher. Additionally, the construction is more aesthetically beautiful with the continuous curving girder. Despite the above-mentioned benefits, horizontally curved girders require more complex analysis and design than straight girders. Because of the girder's curvature, curved girders are susceptible to both vertical bending and torsion [20].

Torsion and distortion from eccentric load are two additional effects that need to be taken into account when using box girders. Components of a general loading on a box girder cause the cross section to twist, bend, and deform. The section twists without the cross section deforming if the torsional component of the loading is applied. There are no transverse flexural distortion stresses produced, and the longitudinal warping stresses are negligible. However, there are additional forces acting on the plate parts if the torsional loading is applied,

and these forces have the tendency to distort the cross section. Transverse distortion stresses and longitudinal warping stresses are produced by the movements of the cross-section's plate parts. However, bending moments, torsional moments, and shear forces are the stress results in a curved beam exposed to gravity loading. While the form of every single stress resultant and the corresponding deformation are quite well defined, under combined stress resultants, the same cannot be stated for any specific type of deformation [21].

Common methods for evaluating torsional deformations during cracking usually involve a computationally-assisted, intricate nonlinear analysis. A wide range of models designed for combined shear, bending, and torsion actions can be used to compute the total nonlinear torsional deformations of concrete beams. To meet the equilibrium and compatibility requirements as well as the material constitutive qualities at any load level, these approaches necessitate gradual and iterative procedures. Thus, from the perspective of practical design, a more precise and efficient way to estimate torsional deformations is required.

Concrete structures with complicated non-linear structural behavior can be effectively and economically analyzed using finite element analysis (FEA). One of the most popular commercial FE software is ABAQUS, which is used here for investigating structural mechanisms and performing parametric studies. More specifically, the behavior of RC horizontally curved deep box girders is numerically modeled using ABAQUS/CAE 2017.

The most accurate way to study structural behavior is through experimental testing, although this approach has many difficulties. The main challenge is that experimental results can vary from one test to another for a variety of reasons. Experimental investigation is also expensive, time-consuming, and constrained. As a result, FE simulation is a useful tool for doing parametric analysis for parameters not taken into account in the experimental program.

There are limitations on treating a horizontally curved bridge as straight in structural design according to the Guide Specifications for Horizontally Curved Bridges. Khalafalla and Sennah [22] found that these limitations are inaccurate when attempting to estimate structural response. This was confirmed by applying finite element modelling (FEM) under dead loading conditions to a number of curved concrete cellular, multi-box, and solid-slab bridge configurations. These members' internal forces were measured and compared to those from straight bridges with comparable designs. When compared to FEM results, the study concluded that the current code constraints for considering curved bridges as straight ones are dangerous. As a result, empirical expressions were created to determine these restrictions with more precision and reliability.

An enhanced finite element analysis (FEA) technique for reinforced concrete (RC) curved box sections was created by Song et al. [23]. This methodology uses curved beam elements at the web-flange joints and curved shell elements for the flanges and webs, combining a layered shell theory approach with orthotropic constitutive models. As a result, less components are required for an accurate simulation. It uses a degenerate superparametric shell element with limited integration to avoid zero-energy modes and shear-locking. To take prestressing forces into account, pre-strain effects are incorporated. Good agreement between the experimental data and the suggested FEA model is seen, especially in terms of stiffness, cracking stresses, and ultimate capacity. Dense reinforcement at flange-web connections and regions with larger cross-sectional area are well-modeled by the hybrid shell and beam element technique.

In the current paper, the results of the FE model will be validated through a comparison with the experimental results of a laboratory specimen. Prior to getting into the details of the created FE model, each component's element, constitutive model types, mesh size, and boundary conditions will be discussed. At last, a parametric analysis will be performed.

Due to the lack of research studying the behavior of deep, horizontally curved box girders, the authors found it necessary for studying. The finite element method was used

due to the quality of its results on the one hand and its low financial and time cost on the other hand, especially when it is available for modeling verification with laboratory results. Accordingly, the effect of significant parameters such as the compressive strength of concrete was studied, as it means to shear resistance in general and strut strength in particular. The whole section width was also studied because it has a direct effect on the resistance to torsional moments, not to mention the width of loading and supporting plates because of its effect on controlling the failure mode.

2. Experimental program

A deep straight (DS) and deep curved (DC), box-girder experimental models were cast and tested for the purpose of verifying the finite element model and comparing the results with the experimental ones. The experimental model has the same dimensions and reinforcement as the numerical model. The curved box girder is 114 degrees was the subtending angle of a circular arc. Pressed cork was used to form the box void along the specimens. The behaviour of the test specimens was examined using two spans, each with a single concentration load. The reinforcement details and fabricated molds are shown in Figure 1.

The specimens are ready for testing by identifying the positions of the load and support points, as shown in Figure. 2. The specimens were tested with a load-controlled testing machine. Three supports that may be positioned on a curved line to support the curved specimen of the current experiment are not provided by the testing apparatus. As a result, a frame with two steel I-sections connecting at a 125-degree angle was particularly manufactured. At the middle of the specimen's span, two LVDTs were fixed in the outer and inner webs. The specimens were subjected to increasing increments of monotonic-static loading until they failed. The test ended when the specimen's total load started to decline.

(a) DS Specimen

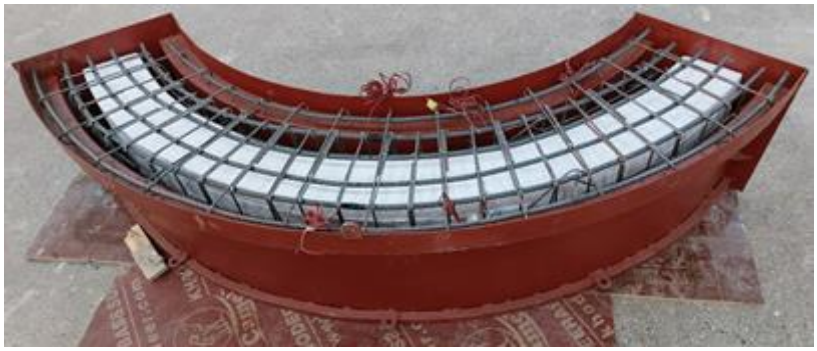

(b) DC Specimen

Figure 1. Reinforcement details and molds of box girders

(a) DS specimen

(b) DC specimen

Figure 2. The geometry, loading condition and cracking patterns of box girders

3. Materials and procedures

3.1 Modelling materials

3.1.1 Concrete

Concrete-damaged plasticity model (CDP) is the failure criterion adopted by ABAQUS. For analysis using CDP, the stress-strain data for concrete are essential. The concrete's ultimate compressive strength was 25 MPa. Concrete behaves linearly within the elastic region until σo = 0.4σu, where, σu= f'c, as shown in Figure 3. In this case, the ultimate strain and peak values were determined to be 0.0019 and 0.0034, respectively. Once concrete reaches this stage, it begins to change plastically, showing some work-hardening up to the ultimate stress and then strain-softening. As suggested in [24–26], various parameters characterizing the CDP were computed. In order to illustrate the inelastic behaviour of concrete, isotropic damaged elasticity in tension and compression was utilized.

For this study, the concrete tensile stress-strain behaviour under uniaxial tensile loading was examined. The concrete in the CDP model has been modelled using the tensile stress-strain as input. Up to the peak, the connection is linearly elastic; beyond that, a postpeak response that softens strain is induced [27].

The suggested values from the studies of other researchers have been used here [28–34] because the computations for these parameters require intricate mathematical derivations and assumptions using the yield surface of the CDP model. By contrasting the numerical results with the experimental data, the modelling was verified. The study's concrete damage parameters are shown in Table 1. The overview of the concrete properties used in the modelling is shown in Table 2. The following are the five parameters that must be defined:

- The dilation angle which represents the ratio of the volume change to shear strain, determined in the plane p − q at high confining pressure where p = − 1/ 3 (2σ1 +σ3) and q = √(3/ 2 (¯s: s)) are the hydrostatic pressure stress and Misses equivalent effective stress respectively and σ1 σ3 are maximum and minimum principal stresses in a triaxial test.

- Eccentricity is a parameter referred to as flow potential eccentricity that defines as the eccentricity tends to zero the flow potential G tends to a straight line (0.1 the default value of eccentricity is used).
- f_{b0}/f_{c0} is the ratio of initial equibiaxial compressive strength to initial uni-axial compressive strength (the default value is used in analysis 1.16).
- k is the ratio of the second stress invariant on the tensile meridian (T.M.) to that on the compressive meridian (C.M.) and it represents the yield surface in the deviatoric plane, and it should satisfy the condition $0.5 < Kc \leq 1.0$
- The viscosity parameter which represents the relaxation time of the viscoplastic system and usually helps improve the rate of convergence of the beam model in the softening region, the viscosity parameter is assumed to be zero because the beam model did not cause severe convergence difficulty. Thus, no viscoplastic regularization is performed in the current analysis.

Table 1: Parameters of concrete damage

Dilation Angle	Eccentricity	f_{b0}/f_{c0}	k	Viscosity
50	0.1	1.16	0.667	0.001

Table 2: Properties of concrete

Modulus of elasticity (MPa)	Poisson ratio	Compressive strength (MPa)	Tensile strength (MPa)
23500	0.2	25	3.25

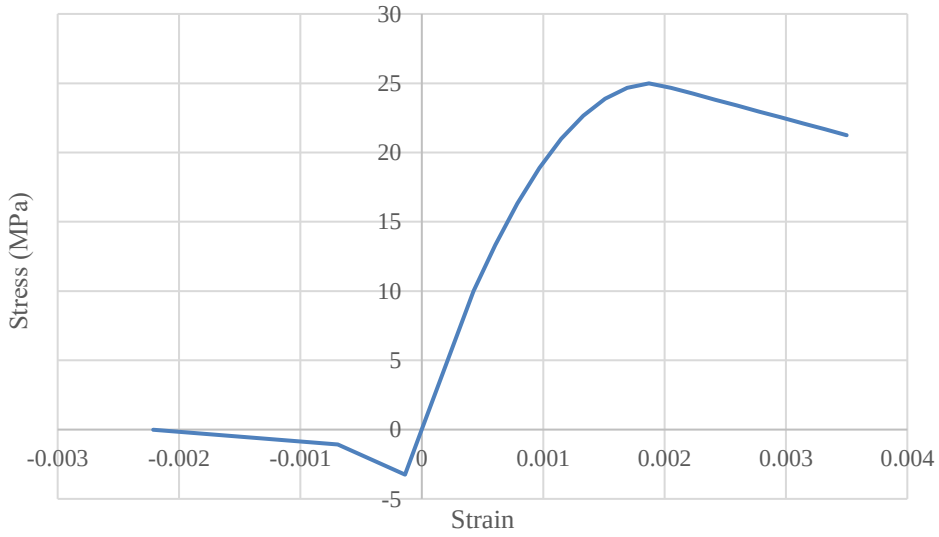

Figure 3. Relationship of stress-strain in compression and tension for concrete

3.1.2 Steel

In the current study, steel reinforcement with a Poisson ratio of 0.3 and elastic modulus of 200000 MPa were used. A 2.5% of the elastic modulus was used for the hardening modulus of elasticity [35]. Table 3 and Figure 4 summarizes the steel properties and its diameter used for the model. Steel is assumed to be an elastoplastic material and identical in compression and tension with a linear elastic response up to yield point and hardening stress from yield point to the ultimate strain.

Table 3: Diameter and properties of steel reinforcements

No.	Diameter (mm)	f_y (MPa)	f_u	Elastic modulus (GPa)
1	12	579	629	200
2	6	474	525	

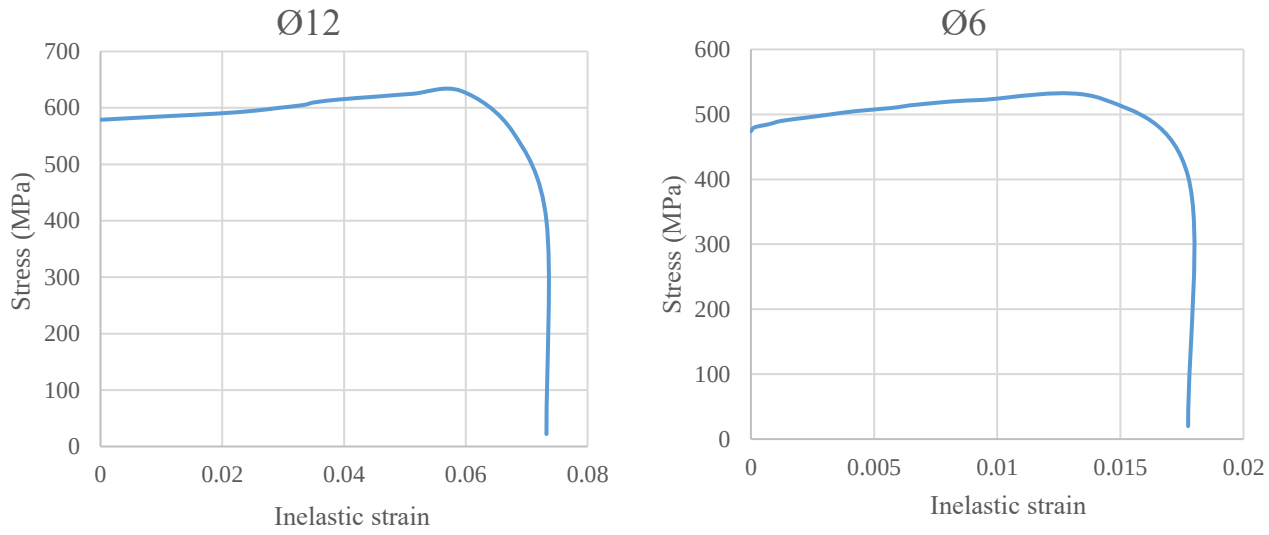

Figure 4. Relationship of stress-inelastic strain in steel reinforcement

3.2 Finite element simulation

Several parts were modelled using the FE simulation software to address the study's objectives. These components include flexure and web reinforcement, as well as concrete plain beams. Eighteen models were taken into consideration for the investigation based on independent variables. Concrete compressive strength, box girder width, and bearing plate width (Lp) for DS and DC box girders were the main parameters in the model. Three dimensional (3D) simulations were used to offer an accurate prediction of the overall behavior and failure process for all RC horizontally curved box girders. The three-dimensional geometry of the FE model prepared for the reference straight and curved specimens are shown in Figure 5. The X-Y plane represents the beam's cross section, while the Z-axis refers to the beam's longitudinal direction. Figure 6 shows the geometric cross section of the box girders. The embedding technique was applied in order to model the type of interaction between the concrete and the reinforcement.

The embedding element in this constraint was chosen to be steel reinforcement bars, while the concrete was represented by the host region. The concrete coming into contact with the loading and supporting plates on one side and the concrete on the other were selected as the interaction features. The mechanical alternatives that were chosen permitted separation following contact and exhibited typical hard contact behavior. Additionally, there is tangential behavior between the two surfaces, with a friction value of 0.35.

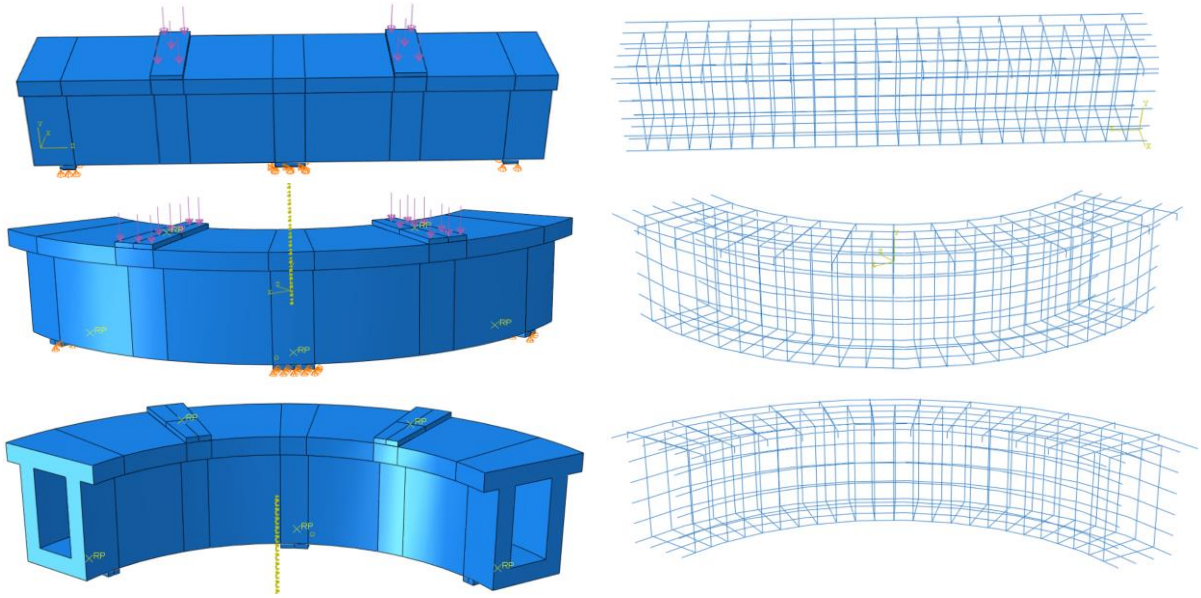

(a) FE model of the concrete **(b)** FE model of the steel reinforcement

Figure 5. 3D finite element modelling of RC straight and curved deep box girders

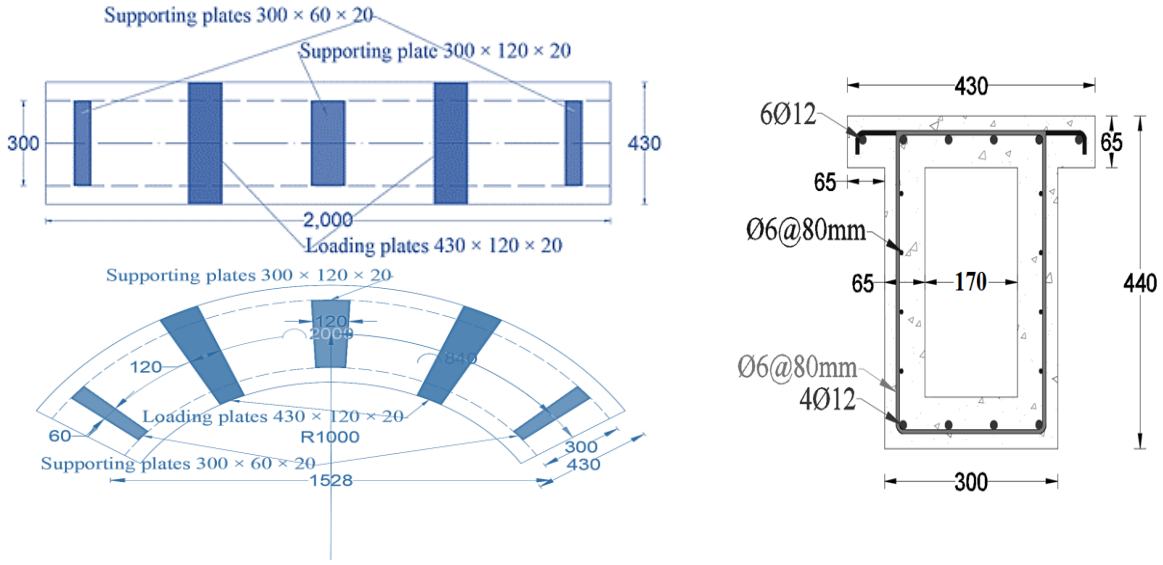

Figure 6. Longitudinal and cross-sectional dimensions of reference straight and curved deep box girders

3.3 Element Type

For solid elements, a three-dimensional eight-node linear brick element with reduced integration (C3D8R) was chosen while utilizing ABAQUS to simulate steel and concrete plates, as shown in Figure 7 (a). This particular element type was selected because it effectively prevents shear-locking phenomena and is appropriate for contact issues. Since reduced integration produces better results and avoids the poor performance that comes with shear locking, it is recommended over full integration. Eight nodes, each with three degrees of freedom, make up each C3D8R element. ABAQUS/standard was used to model the reinforcing bars in RC horizontally curved deep box girders using a linear 3D truss element with two nodes and three degrees of freedom (T3D2), as shown in Figure 7 (b). Truss components embedded in three-dimensional (3-D) continuum brick elements that act as hosts. After the element is embedded, the translational degrees of freedom at its nodes are limited to the proper interpolated values (shape function) in the host continuum element.

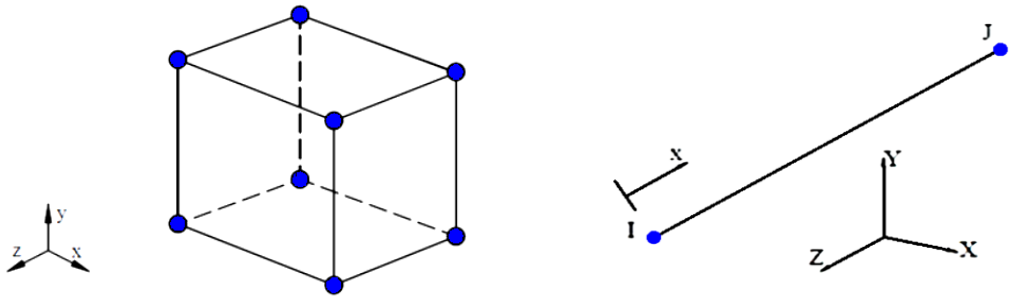

(a) Solid element **(b)** Truss element

Figure 7. Element types in finite element modelling of RC curved deep box girders

3.4 Load and boundary conditions

The load is applied as a pressure load on the top surface of the steel loading plates. To simulate the displacement boundary conditions, the central support was considered as a hinge support (Ux= Uy= Uz = 0), while the edge support plates were restricted in x and y directions (i.e. Ux=Uy=0).

3.5 Mesh size

Many numerical model factors that might influence the prediction of general behavior and ultimate load were studied in this section on the reference specimen. To begin, mesh sensitivity research was conducted to determine the best mesh sizes (30 mm) as shown in Table 4. Based on comparisons between the experimental results and computational efficiency and accuracy, an appropriate mesh size for the curved deep box girder models has been determined. Table 5 displays the number of elements and nodes that were chosen.

Table 4: Results of convergence study

Mesh size (mm)	Deflection of DS Specimen (mm)
40	4
35	4.4
30	5.1
25	5.12

Table 5: Total number of elements and nodes used in the adopted ABAQUS model

Component	No. of Elements	No. of Nodes
Concrete	8772	11937
Steel plates	192	530
Reinforcement	3507	3537

4. Validation of FE model

The experimental results and numerical analysis are compared in terms of load-deflection curves, torsional moment-twisting angle, failure load, and cracking patterns at failure. The theoretical results obtained from the finite element analysis showed a good agreement with the experimental values with a difference of (0.98-0.99), (0.94-0.97) and 1.03 of the experiment for ultimate loading, deflection and twisting angle, respectively. Table 6 summarizes the results of FE analysis and experimental results.

Comparing the experimental and the numerical results, it becomes clear that there is agreement between them on the one hand, and between them and the STM as well on the other hand. Since the stress paths imposed by the STM apply to all of these approaches, that is, the STM imposes that the stresses in deep members are transmitted directly from the loading to the supporting zones, and this is what happened experimentally and numerically as well. It is worth mentioning that the difference in the span length between the outer and inner web was reflected in the experimental, numerical and STM results as well.

Table 6: Summary of the FE results for the specimens

specimen	Result related to	P (kN)	T (kN.m)	FE/Exp.	$P_{cr-diag}$ (kN)	$P_{cr-flex}$ (kN)	Δ (mm)	FE/ Exp.	ψ (degrees)	FE/Exp.
DS	FE	1303	-	0.98	310	320	5.10	0.97	-	-
	Exp.	1332	-		290	300	5.26		-	
DC	FE	1100	16.57	0.99	300	315	8.29	0.94	0.92	1.03
	Exp.	1110	16.72		290	300	8.85		0.89	

4.1 Load-deflection curve

A significant indication of the validity of the FE model is the relationship between the load-deflection and torsional moment-twisting angle, which characterizes the behavior of the members under investigation throughout the loading. Figure 8 and Figure 9 illustrate the load–deflection for reference specimens.

Because no torsional moments were generated in it, the straight specimen showed higher stiffness than the curved specimen, accompanied by no difference in the deflection behavior between the outer and inner web - as happened with the curved specimen.

The results of FEM were compared to the experimental data. The load-deflection and torsional moment-twisting angle predicted by the FEM matched the actual results in most cases. Its response, on the other hand, were stiffer than those obtained from the experimental specimens. The decrease in stiffness results from the cracks, while the ABAQUS software depends on the section as a whole.

The horizontal curvature caused the generation of torsional moments, and their effect was clearly demonstrated experimentally and numerically through the difference in deflection between the outer web and the inner web. The shear dominance made the load-deflection response linear for most of the loading stages, while the appearance of cracks caused the deflection to increase suddenly. In the initial stage, the numerically calculated deflection is consistent with the experimentally measured deflection. This is because, in the elastic stage, the concrete has not cracked, and the sectional stiffness is calculated based on the full section, which is consistent with the finite element analysis results. In the elastic-plastic stage, the concrete constantly cracks and produces many cracks of varying degrees, resulting in a decrease in sectional stiffness.

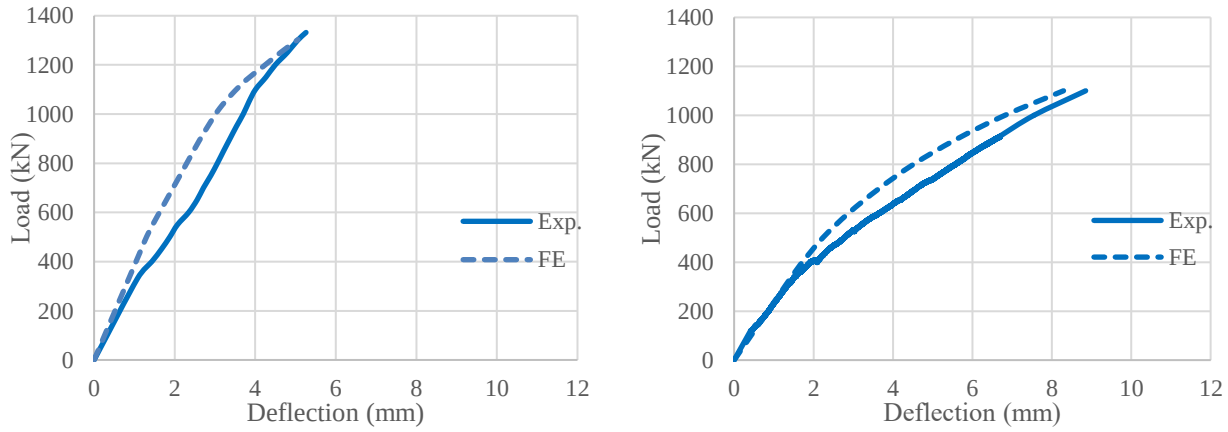

(a) Straight specimen **(b)** Curved specimen

Figure 8. Experimental and numerical load- average deflection curves

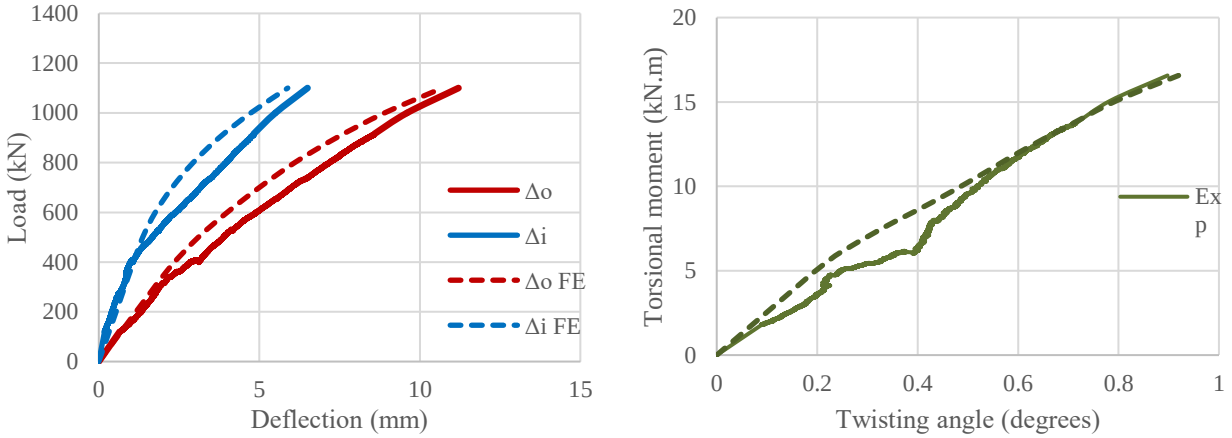

(a) Load-deflection **(b)** Torsional moment-twisting angle

Figure 9. Experimental and numerical deformation curves of curved specimen

4.2 Crack pattern and failure modes

In DS specimen, the first diagonal crack appeared in the middle part of the span between the load and the middle support at about 22%P. With increasing loading, negative flexure cracks appeared in the upper zone near the middle support, and positive flexure cracks appeared in the lower zone near the mid-span, at about 23%P and 31%P, respectively. After that, diagonal cracks appeared in the end part of the span between the load and the end support at about 46%P. These cracks were fewer in number and less developed than those in the middle part of the span.

The cracks resulting from the FEM of DC are similar to experimental cracks, whether in the outer or inner web, as shown in Figure 10. Cracks appeared first in the outer web between the load and the middle support at about 26% of the failure load (P), then in the inner web at about 29%P. Also, flexure cracks appeared first in the negative moment region of the inner web at approximately 27%P, then in the outer web, followed by cracks in the positive moment region at about 40%P. The flexure cracks did not develop much because there was a direct load transition between the supporting points and the loading. That results from the effect of arch action, which takes place due to shear dominance in deep girders. Despite the appearance of cracks, the specimen continued to resist the stresses due to the presence of reinforcing steel that resists the tensile stresses. Finally, the cracks width increased and the specimen failed in diagonal splitting.

It is evident from comparing the experimental and ABAQUS software data that there is convergence in load capacity and behavior. This convergence occurred in the development of cracks and failure mode, where shear behavior dominated in both cases. That is because the height of the specimen relative to span is high. This height led to a direct transfer of stresses between the load and support points on the one hand, and a decrease in bending moments due to small span length on the other hand.

When comparing the straight with the curved specimen, there is no significant difference in behavior, as both are dominated by shear behavior. The cracks and failure mode are the same in both. On the other hand, the straight specimen did not show a difference between the outer and inner web. Experimentally and numerically, the load capacity of the curved specimen was less than the straight one by about 16% and 15%, respectively. Behavior can be divided into several stages:

1. The stage before the appearance of cracks: This is the initial stage of loading in which the stresses resulting from shear forces besides bending and torsional moments are resisted by the linear behavior concrete. Concrete continues to resist the compressive stresses between the load and

the support as well as the resulting perpendicular tensile stresses.

2. The stage of cracks appearance: When the concrete tensile stresses exceed its tension capacity, cracks appear, means that the stresses are transferred from the concrete to the reinforcing steel. A sudden increase in the deflection takes place because the reinforcing steel is more ductile than concrete.
3. The stage of crack development: The number and width of cracks increases, in addition to their extent, depend on the quantity and quality of the available reinforcing steel in addition to its distribution. Loading and deflection continue, cracks develop, and the twist resulting from torsion increases. However, after cracking, a reinforced concrete section behaves nonlinearly; that is, nonlinear methods are needed for analyzing a reinforced concrete beam's response when it is cracked. The structural analysis becomes significantly more complex when nonlinearity is included.
4. Failure stage: When sufficient plastic hinges form to convert a structure into a mechanism with at least one degree of freedom, the structure collapses. If the structure's moment distribution satisfies the requirements of equilibrium, yield, and mechanism all at once, the collapse load is unique.

Numerical methods are considered effective and can produce various results that are difficult to obtain experimentally due to the equipment, cost and time required. It can provide good results when compared to experimental results and then use it to study various parameters to give behavior that can be used to determine the effect and thus obtain a safe design.

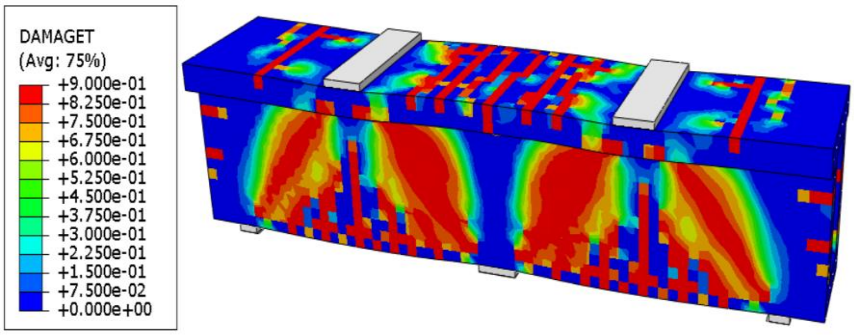

(a) DS specimen

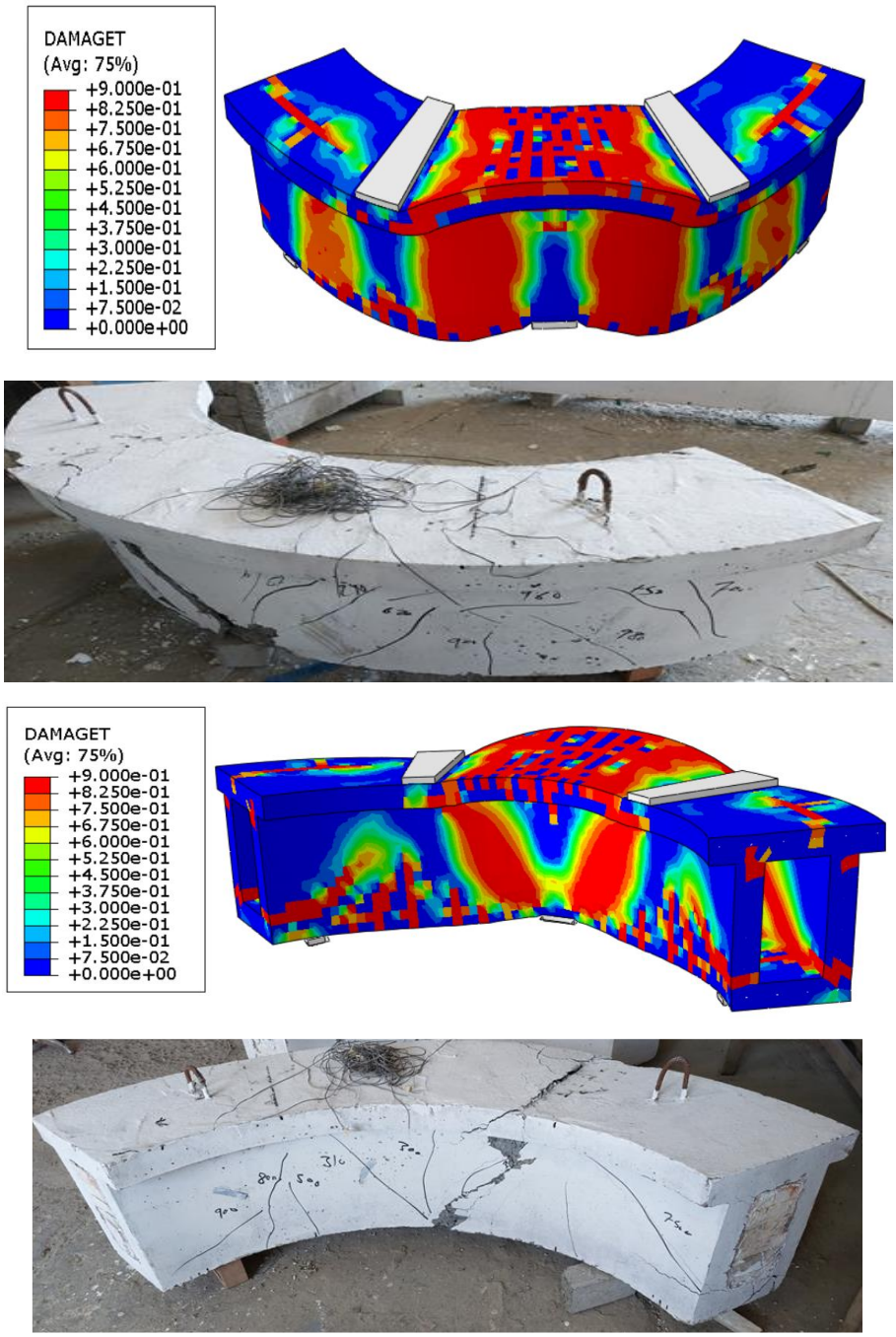

(b) DC specimen

Figure 10. Cracking patterns of finite element model for reference specimens

5. Finite element parametric study

The adopted concrete damaged plasticity model has been thoroughly validated by the FE results shown in the preceding sections. Consequently, parametric studies were carried out to better understand the behavior of continuous curved deep box girders from the perspectives of cost and time savings. In this investigation, three parameters were studied, specifically: concrete compressive strength, total width and the bearing plate width, as shown in Table 7.

Table 7: Geometric dimensions of the box girders

No.	Geometry	Parameter	Length (mm)	Depth (mm)	Web width (mm)	$f'c$ (MPa)	Width (mm)	Bearing plate width (mm)
1	Straight	Reference	2000	440	65	25	300	120
2		$f'c$				35		
3						45		
4						55		
5		width				25	350	
6							400	
7							450	
8		bearing plate width					300	100
9							300	80
10	Curved	Reference				25	300	120
11		$f'c$				35		
12						45		
13						55		
14		width				25	350	
15							400	
16							450	
17		bearing plate width					300	100
18							300	80

5.1. Effect of concrete compressive strength

In the current section, concrete compressive strength values of 25, 35, 45 and 55 MPa were adopted. At the beginning of the load application, varying the concrete compressive strength did not affect the behavior, while with more load application, a slight increase in load capacity and stiffness occurred as shown in Table 8, Table 9, Figure 11 and Figure 12. When the concrete compressive strength became stronger, the ductility decreased and the concrete became more brittle. Increasing the concrete's compressive strength by about 40-120%, increased the load capacity and decreased its deflection by approximately 5-14% and 2-15%, respectively.

Increasing the compressive strength did not show a significant difference at the beginning of the loading because the applied stresses are relatively small, and there are also tensile stresses that are not greatly affected by increasing the compressive strength. The effect increased after the appearance of cracks, as the load and stiffness increased with increasing compressive strength. Increasing the compressive strength causes an increase in the tensile strength, but at high strength concrete the concrete becomes more brittle, so the behavior does not continue at the same pace. At a compressive strength of 55 MPa, the load capacity increased slightly compared to lower values of compressive strength, with a greater decrease in the deflection.

It is true that at the beginning of the load application, the flexural stresses were greater than both the shear and the torsion ones, but they remained a little due to the short span. As loading increased, the shear stresses that normally prevail in deep members increased. These shear stresses are resisted by the concrete and reinforcement, so when the compressive strength of the concrete increased, the shear resistance of the specimen increased.

Table 8: Effect of concrete compressive strength for DS specimen

$f'c$ (MPa)	P_{FE} (kN)	Torsional moment T_{FE} (kN.m)	% Variation in load	Pcr (kN)	Deflection Δ_{FE} (mm)	% Variation in deflection	Twisting angle ψ_{FE} (degrees)	%Variation in Twisting angle
25	1303	-	-	310	5.06	-	-	-
35	1370	-	5.14	326	4.94	-2.37	-	-
45	1449	-	11.20	342	4.76	-5.93	-	-
55	1480	-	13.58	350	4.35	-14.03	-	-

Table 9: Effect of concrete compressive strength for DC specimen

$f'c$ (MPa)	P_{FE} (kN)	Torsional moment T_{FE} (kN.m)	% Variation in load and torsional moment	Pcr (kN)	Deflection Δ_{FE} (mm)	% Variation in deflection	Twisting angle ψ_{FE} (degrees)	% Variation in Twisting angle
25	1100	16.57	-	300	8.29	-	0.92	-
35	1164	17.54	5.82	315	8.01	-3.38	0.89	-3.26
45	1232	18.56	12.00	330	7.67	-7.47	0.85	-7.61
55	1256	18.92	14.18	339	7.05	-14.96	0.79	-14.13

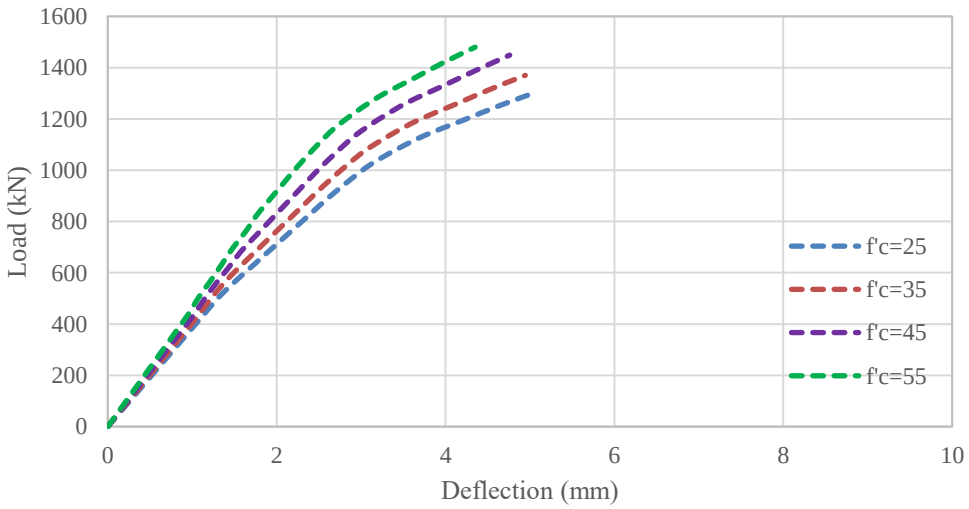

Figure 11. Effect of concrete compressive strength for DS specimen

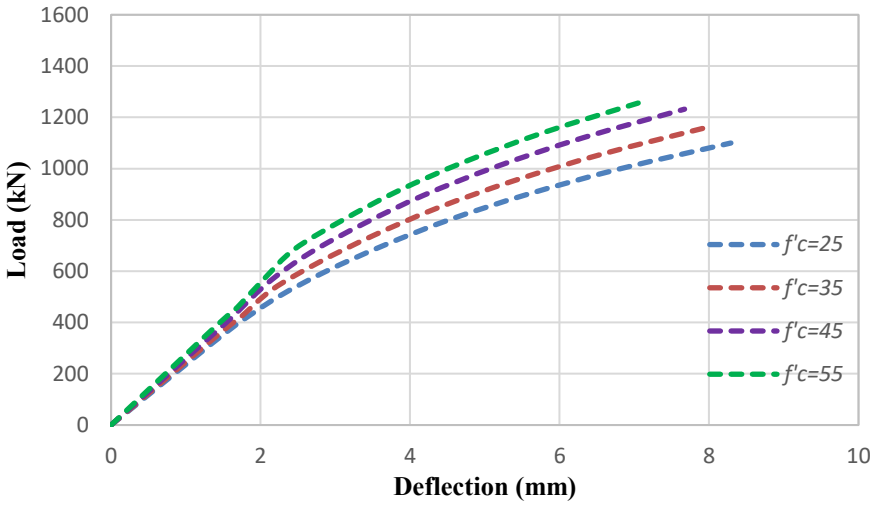

(a) Load-deflection response

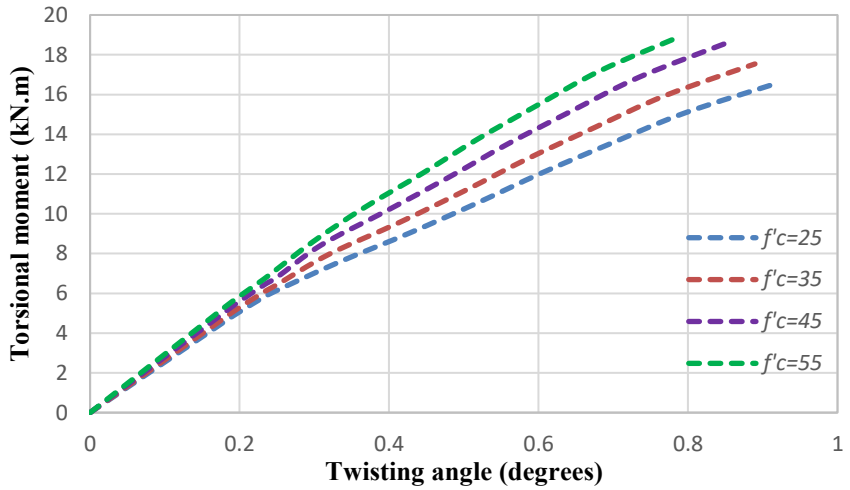

(b) Torsional moment-twisting angle curves

Figure 12. Effect of concrete compressive strength for DC specimen

5.2. Effect of section width

In this section, box girder total width values of 300, 350, 400 and 450 mm were adopted. Increasing the width led to a slight decrease in the load capacity of the box girder as shown in Table 10, Table 11, Figure 13 and Figure 14. By increasing the width of the box girder section, there was an increase in the stiffness. This stiffness increase accompanied by an increase in the resistance of the section to torsional moments, although this increase in section width did not significantly affect the cracking load, load capacity and failure mode.

When the width of the box bridges was increased by about 17-50%, the load capacity did not increase significantly because the shear stresses were transmitted through the web. As for the upper and lower flanges, despite their increased width, the transfer of stress to them is small and within a specific, fixed distance. If the cross section is analyzed separately, increasing the width leads to an increase in the bending moments in the upper flange section at the loading area. It is worth noting that the method of calculating the twist angle changes depending on the width of the box bridge, but as a result it does not differ much because the change in deflection between the outer and inner web is considered relative. The resulting increase in stiffness is the result of an increase in the cross-sectional area, and thus an increase in resistance to torsional moments and a decrease in the twist angle.

Table 10: Effect of box girder width for DS specimen.

Width (mm)	P_{FE} (kN)	Torsional moment T_{FE} (kN.m)	% Variation in load	Pcr (kN)	Deflection Δ_{FE} (mm)	% Variation in deflection	Twisting angle (degrees)	% Variation in Twisting angle
300	1303	-	-	310	5.06	-	-	-
350	1291	-	-0.92	306	4.42	-12.65	-	-
400	1274	-	-2.23	303	3.78	-25.30	-	-
450	1261	-	-3.22	300	3.25	-36.36	-	-

Table 11: Effect of box girder width for DC specimen.

Width (mm)	P_{FE} (kN)	Torsional moment T_{FE} (kN.m)	% Variation in load and torsional moment	Pcr (kN)	Deflection Δ_{FE} (mm)	% Variation in deflection	Twisting angle (degrees)	% Variation in Twisting angle
300	1100	16.57	-	300	8.29	-	0.92	-
350	1079	16.26	-1.91	295	7.18	-13.39	0.80	-13.04
400	1065	16.05	-3.18	290	6.13	-26.06	0.68	-26.09
450	1055	15.90	-4.09	286	5.27	-36.43	0.59	-35.87

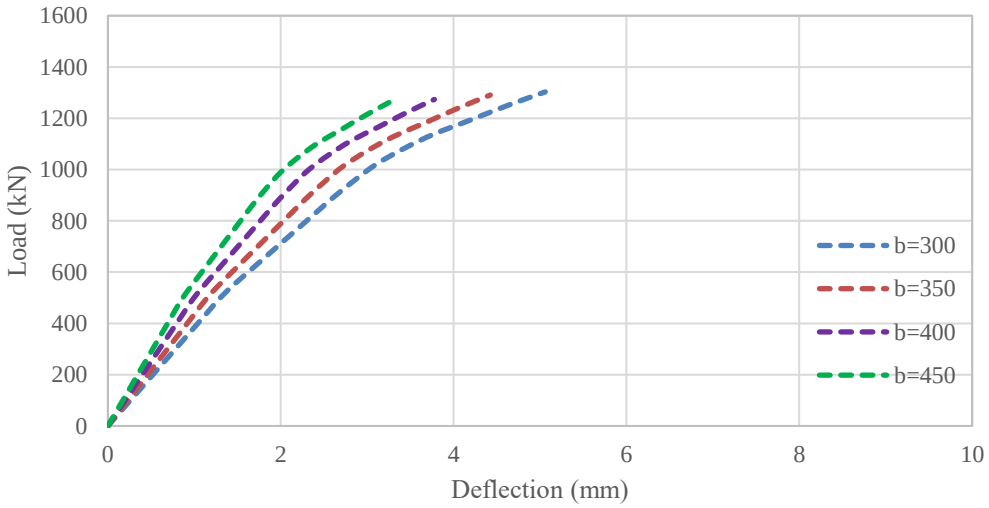

Figure 13. Effect of box girder width for DS specimen

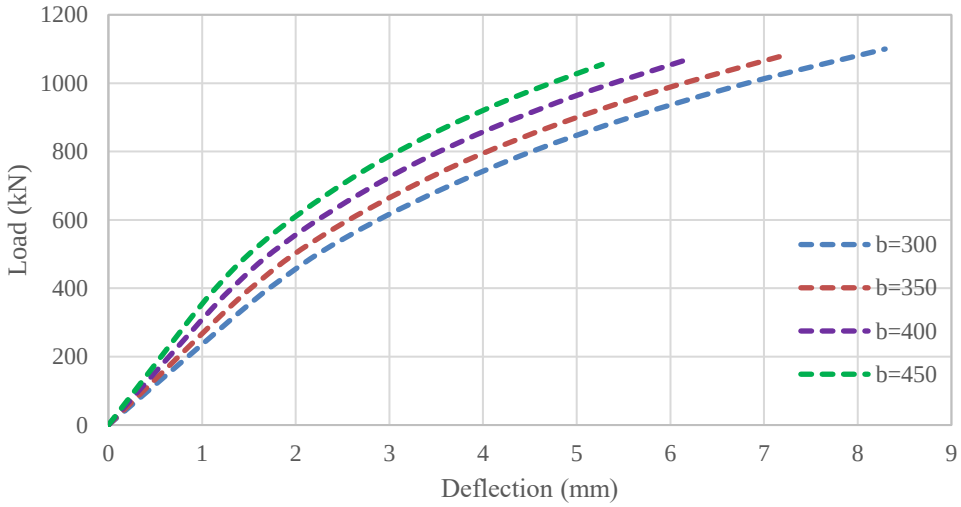

(a) Load-deflection response

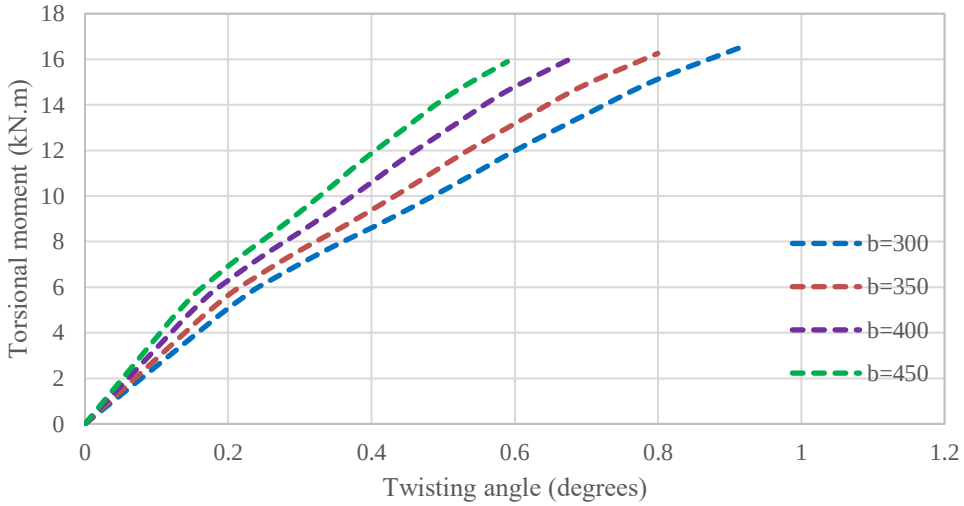

(b) Torsional moment-twisting angle curves

Figure 14. Effect of box girder width for DC specimen

5.3. Effect of bearing plate width

In this section, box girder bearing plate width values (Lp) of 120, 100 and 80 mm were adopted. It is worth to mention that these values indicate the average width of the loading plates and the middle support plate, while the width of the end support plates is half of these values. Decreasing the width of the plates from 120 to 100 mm, i.e. 16.7 %, caused a slight decrease in the load capacity, while the deflection values did not change. Decreasing the width of the plates from 120 to 80 mm, i.e. 33.3 %, causes a greater decrease in load capacity, accompanied by a decrease in stiffness. That took place because failure becomes more brittle as a result of the concentration of stresses in the loading and supporting nodes, as shown in Table 12, Table 13, Figure 15 and Figure 16.

Decreasing the width of the load plates from 120 to 100 did not affect the behavior much, and the failure remained the same, i.e. shear failure. There was a decrease in load capacity and stiffness because the stresses were distributed over a smaller distance and thus were concentrated in the stresses. The final deflection and twist angle were not affected by the decrease in the load plates. When the plate width decreased to 80, there was a greater decrease in load capacity and ductility, the failure became brittle in the loading area. The decrease in the loading area caused a greater concentration of

stresses in the loading area, and thus the concrete failed to resist them and transfer them to the supports. The high depth with less span cause the stresses to be concentrated in the load and support areas, they are not distributed along the span. Therefore, it is important to consider choosing a width of loading plates that can withstand concentrated stresses.

Table 12: Effect of box girder bearing plate width for DS specimen.

Width (mm)	P_{FE} (kN)	Torsional moment T_{FE} (kN.m)	% Variation in load	Pcr (kN)	Deflection Δ_{FE} (mm)	% Variation in deflection	Twisting angle (degrees)	% Variation in Twisting angle
120	1303	-	-	310	5.06	-	-	-
100	1226	-	-5.91	291	5.06	0	-	-
80	1094	-	-16.04	260	4.65	-8.10	-	-

Table 13: Effect of box girder bearing plate width for DC specimen.

Width (mm)	P_{FE} (kN)	Torsional moment T_{FE} (kN.m)	% Variation in load and torsional moment	Pcr (kN)	Deflection Δ_{FE} (mm)	% Variation in deflection	Twisting angle (degrees)	% Variation in Twisting angle
120	1100	16.57	-	300	8.29	-	0.92	-
100	1035	15.59	-5.90	282	8.29	0	0.92	0
80	924	13.92	-16.00	251	7.62	-8.08	0.82	-10.9

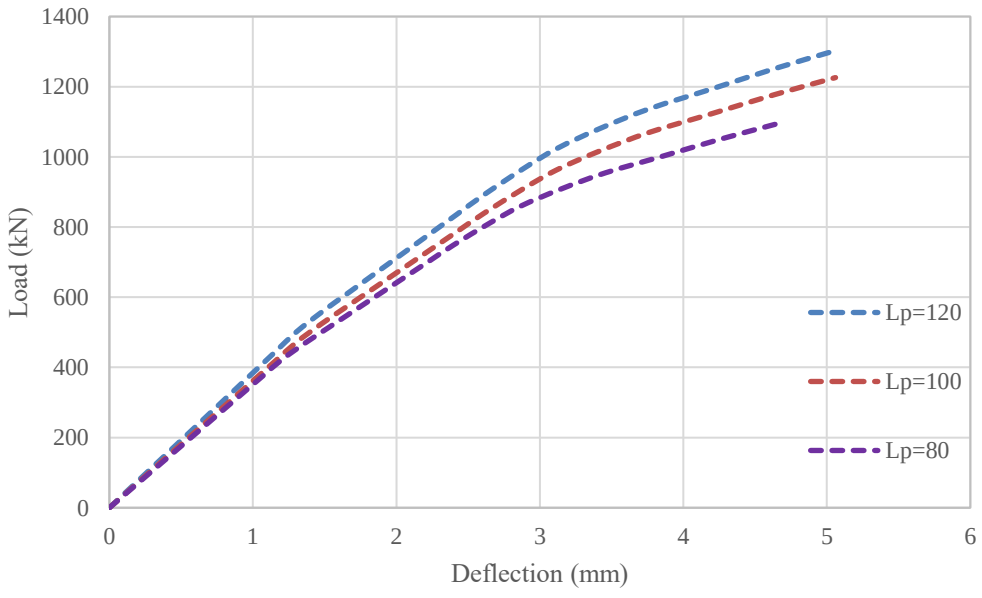

Figure 15. Effect of box girder bearing plate width for DS specimen

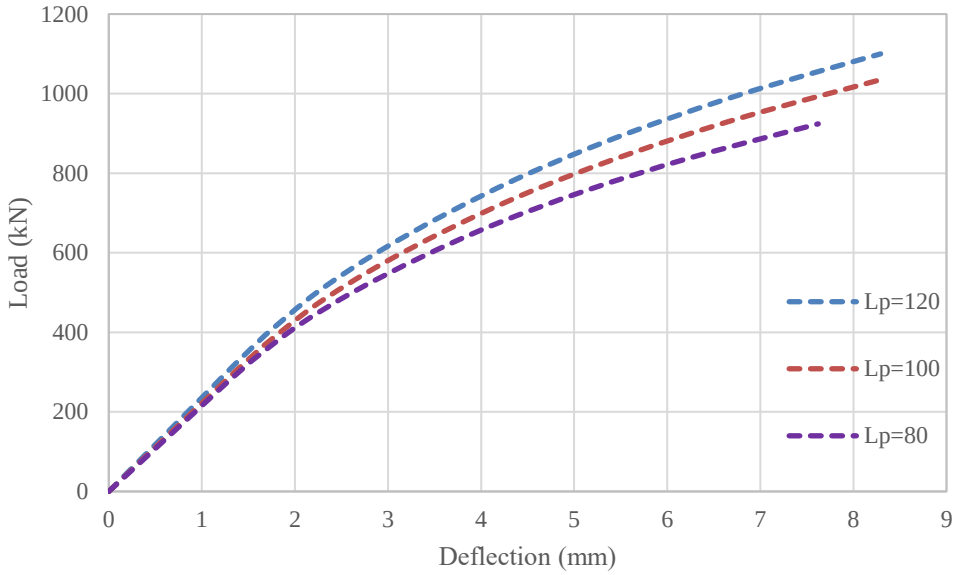

(a) Load-deflection response

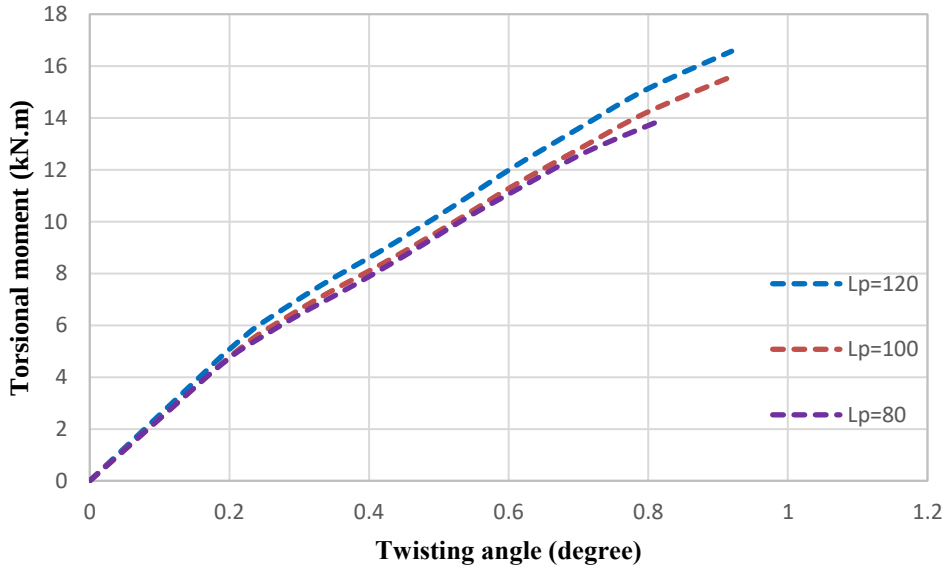

(b) Torsional moment-twisting angle curves

Figure 16. Effect of box girder bearing plate width for DC specimen

6. Conclusions

Because of their higher and varied loads as well as their architectural goals, horizontally curved box bridges are essential. These bridges exhibit complex behaviour due to shear, torsional, and flexural loads. The finite element method (FEM) was applied in order to efficiently examine these parameters. To confirm the accuracy of the numerical model, two deep continuous box girder specimens, one curved and one straight, were cast and put through testing. After verification, a study was carried out on a number of characteristics, such as load plate width, box section width, and compressive strength, which produced important findings.

1. Horizontal curvature generates torsional moments that reduce the box girder's load capacity. On the other hand, increasing height increases resistance to torsion. Therefore, there was no significant

difference between the straight and horizontally curved box girders. The load capacity of the curved specimen was less than the straight one by about 16% and 15% experimentally and numerically, respectively.

2. The finite element modelling within (98-99) % of laboratory models at the load capacity level and (94-97) % of laboratory models at the maximum deflection level, the used modelling demonstrated its value.
3. Increasing the concrete's compressive strength by about 40-120%, increased the load capacity and decreased its deflection by approximately 5-14% and 2-15%, respectively. This is because the high depth causes failure in the struts of the continuous deep box, which is caused by the strength of the concrete.
4. Increasing the width of the deep box section by approximately17-50% did not significantly alter the load capacity level.
5. A reduction of 17-33% in the width of the loading and supporting bearing plates as a result of the stress concentration caused a 6-16% drop in load capacity besides a notable decrease in stiffness. It is important to consider choosing a width of loading plates that can withstand concentrated stresses.
6. It is recommend here using a deep curved box girder when needed to shorten road paths because its load capacity to the torsion generated due to the horizontal curvature makes it close in behavior and load capacity to a straight deep box girder.

References

[1] J. Yuan, L. Luo, Y. Zheng, S. Yu, J. Shi, J. Wang, and J. Shen, "Analysis of the working performance of large curvature prestressed concrete box girder bridges," Materials, vol. 15, no. 15, p. 5414, Aug. 2022.

[2] T. Song, Y. Shen, and G. Li, "Moment redistribution in EPC continuous curved box beams," Journal of Bridge Engineering, vol. 22, no. 8, p. 04017035, 2017.

[3] K. S. Abdul-Razzaq, A. A. Talal, and A. A. Dawood, "The Role of Reinforcement in Concrete Ring Deep Beams," ACI Structural Journal, vol. 120, no. 2, 2023.

[4] K. S. Abdul-Razzaq, W. H. Khaleel, and A. A. Dawood, "Struts and Ties Realization in Reinforced Concrete Ring Deep Beams," ACI Structural Journal, vol. 120, no. 4, 2023.

[5] AASHTO, AASHTO-LRFD bridge design specifications, 8th ed., Washington, DC: American Association of State Highway and Transportation Officials, 2017, 1781 pp.

[6] E. K. Sayhood, R. I. Khalel, and H. M. Hassan, "Load Distribution Factors for Horizontally Curved Concrete Box Girder Bridges," Engineering and Technology Journal, vol. 32, part A, pp. 748-762, 2014.

[7] M. A. Hadi, E. K. Sayhood, and A. S. Resheq, "Shear strength of reinforced fibrous-self compacted concrete box girder using recycled concrete aggregate," Engineering and Technology Journal, vol. 39, no. 8, pp. 1307-1320, 2021.

[8] R. N. Abood, K. S. Abdul-Razzaq, and A. K. Kadhum, "Pure Effect of Temperature on Rectangular and Trapezoidal Box-Girder Bridges–A Finite Element Investigation," Diyala Journal of Engineering Sciences, vol. 17, no. 1, pp. 124-140, 2024.

[9] T. S. Al-Attar, S. S. Abdul Qader, and H. A. Hussain, "Torsional behavior of solid and hollow core self compacting concrete beams reinforced with steel fibers," Engineering and Technology Journal, vol. 37, no. 7A, pp. 248-255, 2019.

[10] R. Gaspar and F. R. Stucchi, "Web design of box girders concrete bridges," Engineering Structures, vol. 57, pp. 267-275, Dec. 2013.

[11] A. H. Nilson, D. Darwin, and C. W. Dolan, Design of Concrete Structures, 14th ed., New York, NY, USA: McGraw-Hill Companies, Inc, 2009.

[12] ACI Committee 318, Building Code Requirements for Structural Concrete, Hills, MI, USA: ACI, 2019.

[13] Q. M. Shakir and H. K. Hannon, "Innovative model of precast RC curved hybrid deep beams composed partially with high-performance concrete," Arabian Journal for Science and Engineering, vol. 49, no. 4, pp. 6045-6060, 2024.

[14] Q. M. Shakir and H. K. Hanoon, "Behavior of high-performance reinforced arched-hybrid self-compacting concrete deep beams," Journal of Engineering Science and Technology, vol. 18, no. 1, pp. 792-813, 2023.

[15] G. Kenea, "Analytical study of geometric parameter effect on the behavior of horizontally curved reinforced concrete deep beam," Journal of Engineering, vol. 2022, 2022.

[16] E. K. Sayhood, A. S. Resheq, and A. J. Habeeb, "Shear strength of concrete deep beam subjected to uniformly distributed load," Engineering and

Technology Journal, vol. 36, no. 2A, pp. 125-135, 2018.

[17] N. A. Al-Bayati, B. R. Muhammed, and M. F. Oda, "Effect of shear span to effective depth ratio on the behavior of self-compacting reinforced concrete deep beams containing openings strengthened with CFRP," Association of Arab Universities Journal of Engineering Sciences, vol. 26, no. 1, pp. 1-9, 2019.

[18] A. A. Dawood and K. S. Abdul-Razzaq, "Shear Friction and Strut-and-Tie Modeling Verification for Pier Caps," Journal of Bridge Engineering, vol. 26, no. 9, p. 04021059, 2021.

[19] K. S. Abdul-Razzaq, A. M. Jalil, and A. A. Dawood, "Reinforcing struts and ties in concrete continuous deep beams," Engineering Structures, vol. 240, p. 112339, 2021.

[20] A. A. Dawood, K. S. Abdul-Razzaq, and W. S. Abdulsahib, "Torsional Strength of Horizontally Curved Continuous Reinforced Concrete Box Girder Bridges," Engineering and Technology Journal, pp. 1-12, 2023.

[21] B. Kermani and P. Waldron, "Analysis of continuous box girder bridges including the effects of distortion," Computers & Structures, vol. 47, no. 3, pp. 427-440, 1993.

[22] I. E. Khalafalla and K. Sennah, "Curvature limitations for concrete box-girder and solid-slab bridges," ACI Structural Journal, vol. 111, no. 5, p. 1003, 2014.

[23] T. Song, C. S. W. Yang, D. W. Scott, Y. Shen, and G. Li, "Novel finite element analysis of curved concrete box girders using hybrid box elements," Journal of Structural Engineering, vol. 147, no. 1, p. 04020284, 2021.

[24] Y. Sümer and M. Aktas, "Defining parameters for concrete damage plasticity model," Challenge Journal of Structural Mechanics, vol. 1, no. 3, pp. 149-155, 2015. doi:10.20528/cjsmec.2015.03.005

[25] A. Hamicha and G. Kenea, "Investigation on the effect of geometric parameter on reinforced concrete exterior shear wall-slab connection using finite element analysis," Advances in Civil Engineering, vol. 2022, Article ID 4903650, 17 pages, 2022.

[26] E. Megarsa and G. Kenea, "Numerical investigation on shear performance of reinforced concrete beam by using ferrocement composite," Mathematical Problems in Engineering, vol. 2022, Article ID 5984177, 12 pages, 2022.

[27] ABAQUS, ABAQUS 6.14, Providence, RI, USA: ABAQUS, 2014.

[28] R. Malm, G. S. James, and H. Hakan, "Monitoring and evaluation of shear crack initiation and propagation in webs of concrete box-girder sections," in Proceedings of the International Conference on Bridge Engineering—Challenges in the 21st Century, Hong Kong, China, 2003.

[29] J. Lee, G. L. Fenves, and M. Asce, "Plastic-damage model for cyclic loading of concrete structures," Journal of Engineering Mechanics, vol. 124, no. 8, pp. 892-900, 1998.

[30] W. Ren, L. H. Sneed, Y. Yang, and R. He, "Numerical simulation of prestressed precast concrete bridge deck panels using damage plasticity model," International Journal of Concrete Structures and Materials, vol. 9, no. 1, pp. 45-54, 2015.

[31] H. Kupfer, H. Hilsdorf, and H. Rusch, "Behaviour of concrete under biaxial stresses," International Concrete Abstracts Portal, vol. 66, no. 8, pp. 656-666, 1969.

[32] J. Lubliner, J. Oliver, S. Oller, and E. Onate, "A plastic-damage model for concrete," International Journal of Solids and Structures, vol. 25, no. 3, pp. 299-326, 1989.

[33] A. Feyissa and G. Kenea, "Performance of shear connector in composite slab and steel beam with reentrant and open trough profiled steel sheeting," Advances in Civil Engineering, vol. 2022, Article ID 5010501, 14 pages, 2022.

[34] M. Z. Kareem, Q. W. Ahmed, and U. M. Salih, "Finite Element Investigation of the Ultimate Capacity of FRP Strengthening Soffit Curved Girders," Diyala Journal of Engineering Sciences, vol. 17, no. 1, pp. 75–83, 2024.

[35] A. A. Al-Manaseer and D. V. Phillips, "Numerical study of some post-cracking material parameters affecting nonlinear solutions in RC deep beams," Canadian Journal of Civil Engineering, vol. 14, no. 5, pp. 655-666, 1987.